5SWC0 - Linear and Planar Motors for High-precision Systems

Lab Assignment Group 1

J.M. van Dam (ID: 0806678)
j.m.v.dam@student.tue.nl
Department of Mechanical Engineering

M. Kleijer (ID:0813485)
m.kleijer@student.tue.nl
Department of Electrical Engineering

January 16, 2018

1. Introduction

For the course 5SWC0 Linear and Planar Motors for High-precision Systems students are asked to combine the knowledge provided during the lectures with hands-on experience on an actual linear motor via several experiments. These experiments include measurements of EMF, phase resistances, phase inductances and disturbances to identify parameters of a iron core linear motor. Additionally, the experiments will explore current commutation as well as the implementation of a feed-forward control loop. The machine set consists of a iron core linear motor that is coupled to:

- A power amplifier for actuation of the machine
- A LCR meter to measure resistances and inductances
- The dSpace system for measurements of EMF, position, velocity, etc.

In the coming pages of the report the procedures and findings during the measurements are described.

2. EMF

In the first experiment, the set-up has no external excitation, except for the manual pushing of the actuator. This means that the voltage measured with the dSpace systems equals the induced EMF.

2.a. Question 1

It is known that the voltage is measured line-to-line and that it equals the induced EMF

$$EMF = \frac{d\phi}{dt} = \frac{d\phi}{dx}v. \tag{1}$$

where ϕ is the change of flux versus either time or position and v is the speed of the translator. As the EMF is measured line-to-line, it is transformed to phase EMF by dividing with $\sqrt{3}$. Additionally, as the speed of the translator was also measured, a plot for the EMF as a function of position at a speed of 1 m/s via

$$\frac{d\phi}{dx} = \frac{EMF}{v}, \tag{2}$$

is realized. Fig. 1 depicts the transformed EMF waveform of one of the phases.

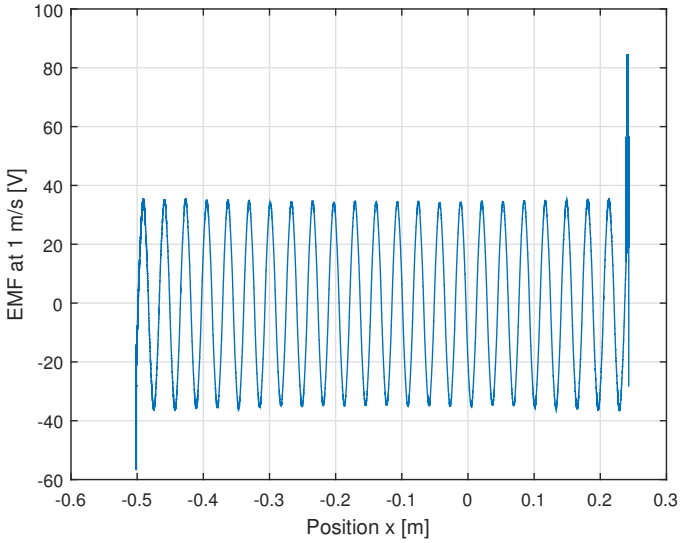

Figure 1: Phase EMF as a function of position at a speed of 1 m/s for one phase

2.b. Question 2

From the waveform illustrated in Fig. 1 one can find the pole pitch τ, which is the distance between two magnets, by finding the length of half a period of the EMF waveform. Hence, the pole pitch equals 16 mm.

2.c. Question 3

Additionally, from Fig. 1 one can derive the motor constant

$$K_t = \frac{3}{2} EMF_{pk}, \tag{3}$$

where EMF_{pk} is the peak value of the EMF waveform. By extracting the peak values of the EMF via Fig. 1 the motor constant is found to be 54.18 N/A_{pk}. Furthermore, by dividing this value with $\sqrt{2}$ one will find a motor constant of 38.31 N/A_{RMS}.

2.d. Question 4

Finally, in Fig. 2 the transformed EMF waveform of both phases is given. The only difference that is noted between the two is the phase shift between the phases. A difference in peak magnitudes is possible due to a slight difference in phase parameters, as will be discussed in the next experiment, or due to one of the phases experiencing more end effects due to the position of the winding in the motor, but no difference in EMF magnitude is noticeable.

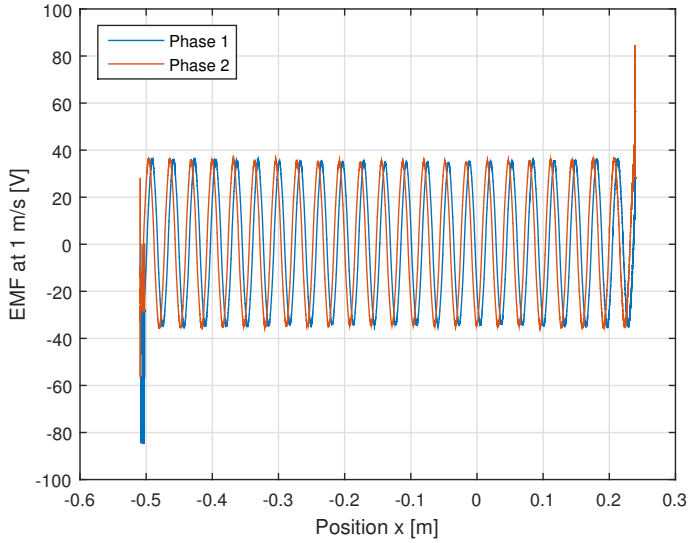

Figure 2: Phase EMF as a function of position at a speed of 1 m/s for two phases

3. Phase resistances

In this experiment the phase resistances of the machine set are measured with the LCR meter.

3.a. Question 5

Due to the star connection of the windings, the individual resistances cannot be measured directly. However, the combined resistances $R_a + R_b$, $R_b + R_c$ and $R_a + R_c$ can be measured with the LCR meter. The resulting values are 3.76Ω, 3.54Ω and 3.65Ω, respectively. Now, the individual phase resistance for R_a, R_b and R_c can be calculated, which equal 1.935Ω, 1.825Ω and 1.715Ω. As the phase resistances are assumed equal the magnitude of 1.825Ω is selected to be the final phase resistance.

4. Phase inductances

Next, the LCR meter is used to measure the phase inductances.

4.a. Question 6

The values for the phase inductances L_a, L_b and L_c are found to be 31.93 mH, 26.06 mH and 26.72 mH, respectively.

4.b. Question 7

Removing the magnets from the motor will have negligible effect on the inductance

$$L = \frac{d\lambda}{di} = \frac{N^2}{R_{tot}}, \tag{4}$$

as the permeability of the magnets is almost equal to the permeability of the air. Here, λ is the flux linkage, N the number of turns of the winding and R_{tot} the total reluctance of the system. Since the permeability of the magnets equals that of the air the total reluctance will not change when removing the magnets. Additionally, the number of turns also remains equal. Hence, inductance does not change when the magnets are removed.

4.c. Question 8

The phase inductances can be written as:

$$L_a = L_{aa} + L_{bb} + 2M, \tag{5}$$

$$L_b = L_{bb} + L_{cc} + 2M, \tag{6}$$

$$L_c = L_{aa} + L_{cc} + 2M. \tag{7}$$

where L_{aa}, L_{bb} and L_{cc} are the self inductances and M the mutual inductance. This makes clear that the mutual inductance cannot be obtained from this measurement.

5. Friction force

For this experiment the machine is actuated with certain motion profiles from which the static friction or Coulomb friction and dynamic friction or damping can be derived. The motor constant calculated via the EMF measurements is implemented into the dSpace measurement environment.

5.a. Question 9

The total friction force

$$F_{friction} = sign(v)F_{Coulomb} + Dv, \tag{8}$$

consists of Coulomb friction and damping. Here, $F_{Coulomb}$ is the magnitude of the Coulomb friction and D the damping coefficient. By assuming some values, one is able to create a sketch for the friction force as function of the velocity. Fig. 3 shows the aforementioned sketch. To obtain the actual values for the Coulomb friction and the damping coefficient one should apply a motion profile in order to accelerate the machine to a particular speed level as quickly as possible, followed by maintaining this speed at a constant level until the machine has to come to a standstill, which has to decelerate as quickly as possible.

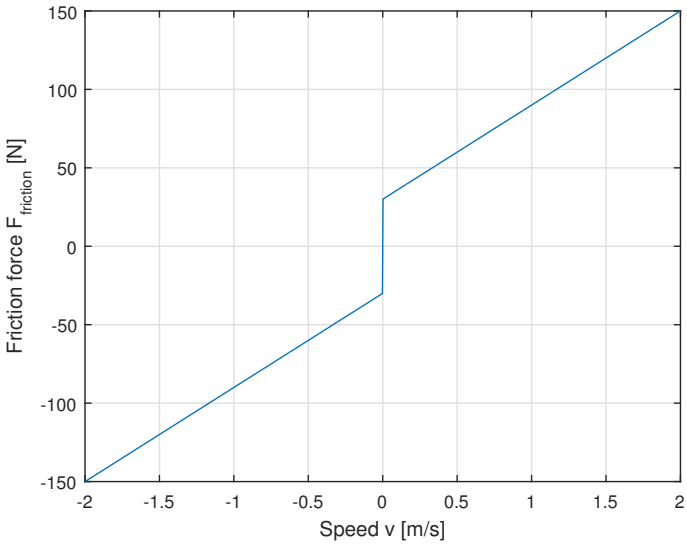

Figure 3: Sketch of the friction force as a function of velocity

The required motion profile is thus shaped like a trapezoidal. Acceleration and deceleration should be maximum as one needs constant velocity for different velocity levels to obtain the parameters. The next two questions will discuss these measurements and the corresponding calculations of the Coulomb friction and damping coefficients.

5.b. Question 10

The motion profile discussed earlier is applied to the system for six different speed levels. The speed levels considered are relatively high, because this will limit the cogging force effect. Additionally, the corresponding force measurements are only observed for the constant speed periods (meaning that the acceleration and deceleration parts are filtered out) as the resulting force is then zero. Now, the measured force can be assumed to equal the friction force. Fig. 4 depicts the mean friction force points for the different speeds, as well as the linear fit through these points.

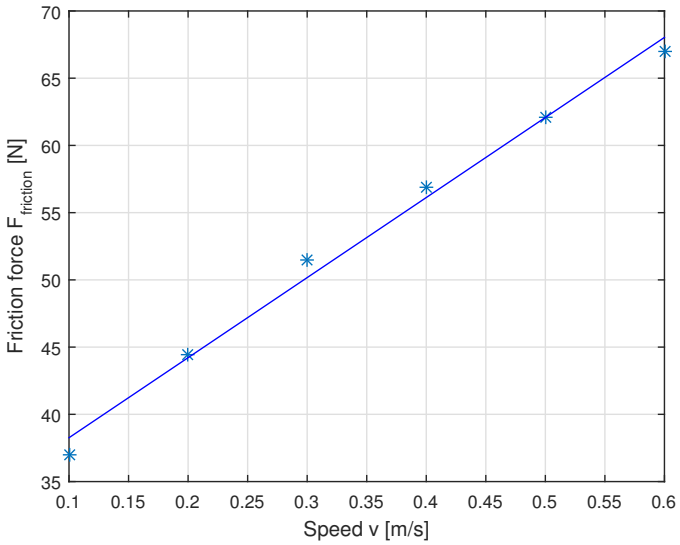

Figure 4: Mean friction force for different speed levels together with its linear fit

5.c. Question 11

From the linear fit of Fig. 4 the friction parameters are found to be 32.31 N for the Coulomb friction and 59.54 for the damping coefficient.

6. Cogging force

Besides the friction force, the cogging force also acts as a disturbance force. The latter has yet to be mapped, which is done in this experiment.

6.a. Question 12

The frequency of the cogging force one could expect for a speed of 1 m/s is

$$f = \frac{v}{\tau} = \frac{1}{16e^{-3}} = 62.5Hz. \tag{9}$$

6.b. Question 13

To measure the cogging force one needs the same motion profile as for the friction measurements, however, the speed should be lower as this will cause the cogging effect to be more severe and, therefore, better noticeable. Furthermore, question 12 illustrates that the cogging force frequency at a speed of 1 m/s exceeds the bandwidth of 50Hz of the controller. This means that the maximum speed that can be used for the cogging force measurements equals

$$v = f\tau = 50x16e^{-3} = 0.8m/s. \tag{10}$$

Nevertheless, as one uses a low speed for the measurement this aspect is not a problem.

6.c. Question 14

As will be discussed later the measured cogging force is used for a feed-forward controller after some filtering. However, the initial selected speed of 0.01 m/s gave problems during the filtering for the look-up table as with such a low speed the dSpace gives too much data for the filter too handle. Therefore, a higher speed of 0.5 m/s was used for the cogging force measurements. Fig. 5 shows the measured cogging force, obtained from subtracting the friction forces from the measured force. This data was then filtered to a 2000 point look-up table, which will be used for the feed-forward controller. Fig. 6 depicts the cogging force that is used for the look-up table after the filtering of the original data. Furthermore, it can be noted that the cogging force is very high during acceleration and deceleration, so to properly visualize the cogging force during motion with constant velocity, Fig. 7 provides a zoom-in of the cogging force over position of the linear motor. The high peak of the force during acceleration and deceleration is caused by the fact that friction forces and mass acceleration are not modeled for this kind of motion, meaning that the cogging force measurement is off.

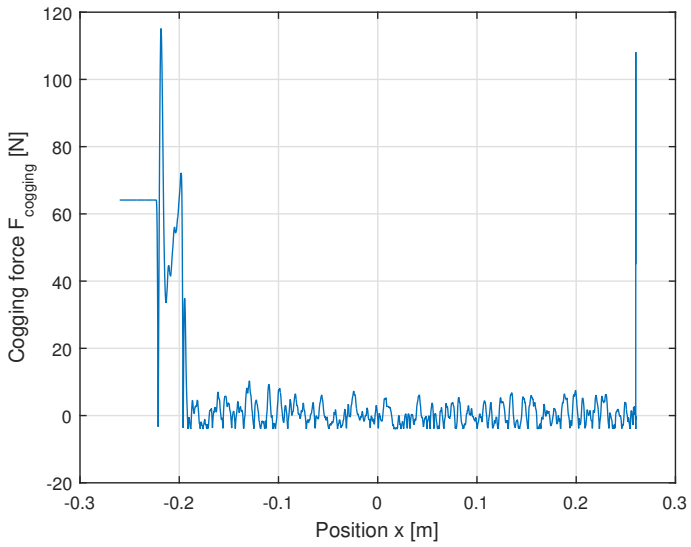

Figure 5: Measured cogging force versus position over the linear motor

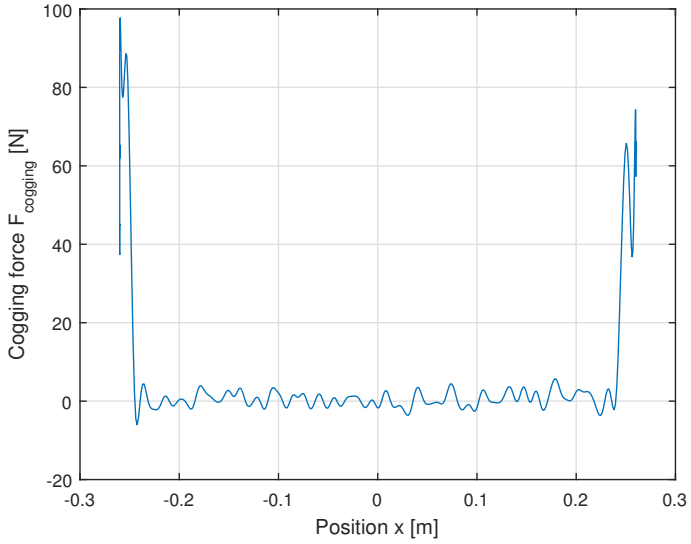

Figure 6: Filtered cogging force versus position over the linear motor

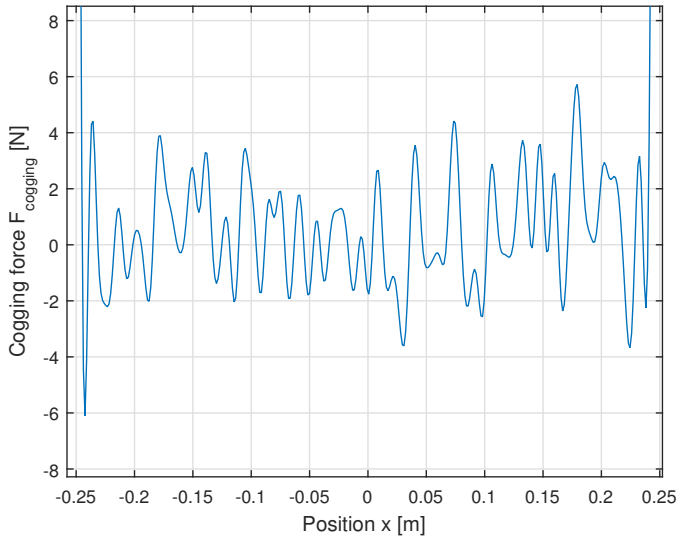

Figure 7: Zoom-in of the filtered cogging force versus position over the linear motor

7. Commutation angle

In this experiment the effect of a phase error with respect to the optimum commutation angle on the force production of the linear motor is investigated; it is known that a perpendicular commutation angle is most efficient.

7.a. Question 15

First, a visualization of the phase currents for zero error in the commutation angle is made. The measurement environment of dSpace tracks two of the three phase currents. The third phase current can then be derived via:

$$i_a + i_b + i_c = 0. \tag{11}$$

Fig. 8 shows the phase currents during the provided motion profile.

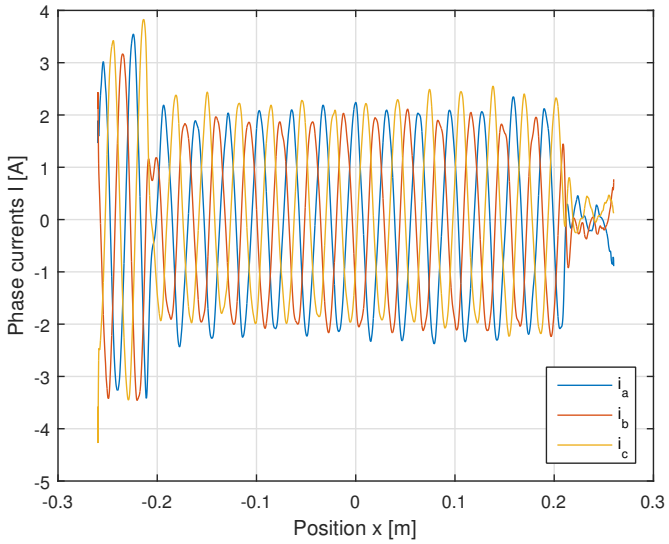

Figure 8: Phase currents during the provided motion over the linear motor

7.b. Question 16

Now, the current measurements are repeated for different phase angle errors. The average peak value for one of the phase currents is tracked and divided by $\sqrt{2}$ to get the RMS current for different phase errors. Fig. 9 illustrates the effect of the error in the commutation angle on the RMS current. Additionally, the energy dissipated in the windings

$$W_d = 3I_{rms}^2 R_{ph}, \tag{12}$$

has the same shape. Here, I_{rms}^2 is the aforementioned RMS current and R_{ph} is the phase resistance. Fig. 10 shows the energy dissipated in the windings versus the phase angle error.

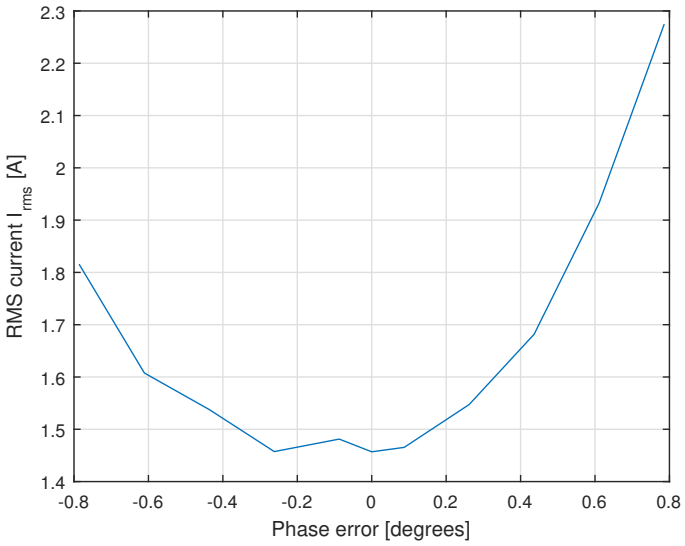

Figure 9: RMS current versus phase angle error

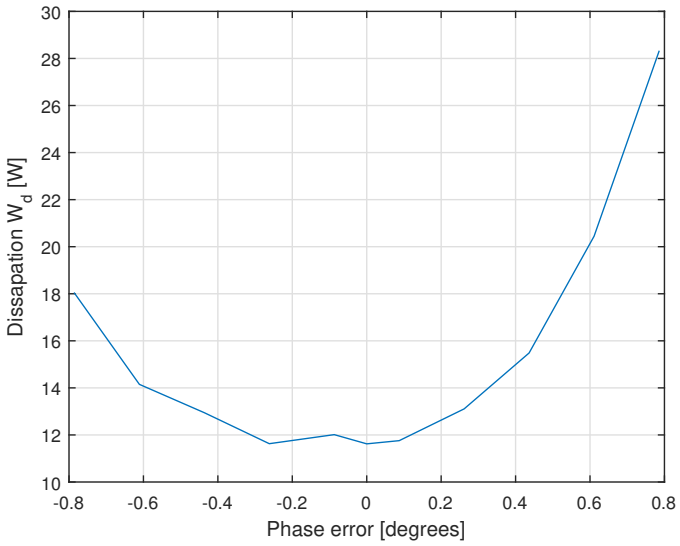

Figure 10: Energy dissipation in the windings versus phase angle error

7.c. Question 17

From the last two questions it becomes clear that the error in the ideal commutation angle results in higher RMS currents, therefore, higher losses in the windings and, hence, less force production. In other words, the machine constant becomes lower.

8. Feed-forward controller

Finally, the filtered waveform for the cogging force is applied to the look-up table for the provided feed-forward controller. The effect of such a controller is investigated during this experiment.

8.a. Question 18

Fig. 11 shows the effect of the implementation of the feed-forward controller. By adding feed-forward to the controller, the error during acceleration and deceleration is greatly decreased. Also, during constant movement the error is slightly better using feed-forward, as the cogging is then countered. However, the biggest error after implementing feed-forward still occurs during the acceleration and deceleration, as was already observed during the cogging measurements.

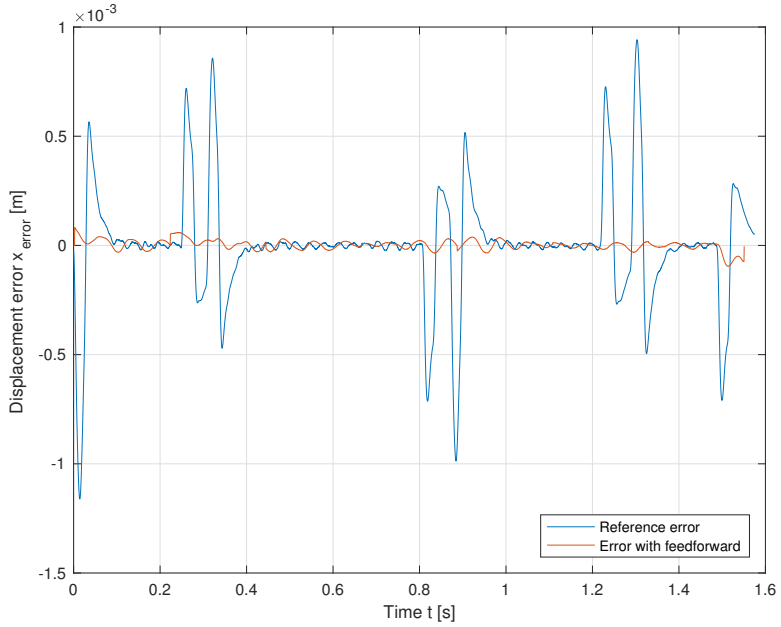

Figure 11: Error of reference (blue) compared with use of feed-forward (red)